fibers

MDPI

Article

Structural Health Monitoring of Partially Replaced Carbon Fabric-Reinforced Concrete Beam

Ramalingam Malathy [1,*], Jenifar Monica James [1], Mayakrishnan Prabakaran [2,3,*] and Ick Soo Kim [4,*]

[1] Department of Civil Engineering, Sona College of Technology, Salem 636005, India
[2] Institute for Fiber Engineering and Science (IFES), Interdisciplinary Cluster for Cutting Edge Research (ICCER), National University Corporation Shinshu University, Nagano 386-8567, Japan
[3] Department of Biomaterials, Saveetha Dental College and Hospitals, SIMATS, Saveetha University, Chennai 600077, India
[4] Nano Fusion Technology Research Lab, Interdisciplinary Cluster for Cutting Edge Research (ICCER), Division of Frontier Fibers, Institute for Fiber Engineering (IFES), Shinshu University, Nagano 386-8567, Japan
* Correspondence: malathycivil@sonatech.ac.in (R.M.); prabakarannitt@gmail.com (M.P.); kim@shinshu-u.ac.jp (I.S.K.)

Abstract: Textile-reinforced concrete (TRC) is a composite concrete material that utilizes textile reinforcement in place of steel reinforcement. In this paper, the efficacy of the partial replacement of steel reinforcement with textile reinforcement as a technique to boost the flexural strength of reinforced concrete (RC) beams was experimentally investigated. To increase the tensile strength of concrete, epoxy-coated carbon textile fabric was used as a reinforcing material alongside steel reinforcement. Beams were cast by partially replacing the steel reinforcement with carbon fabric. Partially replaced carbon fabric-reinforced concrete beams of size 1000 × 100 × 150 mm^3 were cast by placing the fabrics in different layers. A four-point bending test was used to test cast beams as simply supported until failure. Then, 120 ohm strain gauges were used to study the stress–strain behavior of the control and TRC beams. Based on this experimental study, it was observed that 50% and 25% of the steel replaced with carbon fabric beams performed better than the conventional beam. ABAQUS software was used for numerical investigation. For the load deflection characteristics, a good agreement was found between the experimental and numerical results. Based on the experimental analysis carried out, a prediction model to determine the ultimate load-carrying capacity of TRC beams was created using an Artificial Neural Network (ANN).

Keywords: textile-reinforced concrete; carbon fabric; tensile strength; four-point bending; flexural behavior; ANN

Citation: Malathy, R.; James, J.M.; Prabakaran, M.; Kim, I.S. Structural Health Monitoring of Partially Replaced Carbon Fabric-Reinforced Concrete Beam. *Fibers* **2024**, *12*, 67. https://doi.org/10.3390/fib12080067

Academic Editor: Dae-jin Kim

Received: 19 February 2024
Revised: 5 July 2024
Accepted: 15 July 2024
Published: 21 August 2024

1. Introduction

Steel-reinforced concrete is one of the most important building materials used in the construction industry [1]. The carbonization of concrete and corrosion of reinforcing steel due to air exposure results in a reduction in the strength and durability of the structure [2]. Thus, non-corrosive materials have become more significant during the past three decades as precast and lightweight concrete constructions with great durability have been a priority [3]. High-performance fibers implanted in the shape of a textile mesh are combined with conventional concrete to create textile-reinforced concrete (TRC) [4,5]. It is intended to improve the concrete's mechanical properties, including tensile strength, ductility, and impact resistance, which are typically low in conventional concrete [6–11].

In TRC, the textile reinforcement serves as a replacement for traditional steel reinforcement, offering advantages like corrosion resistance, ease of handling and installation, and improved crack control [12,13]. The process of manufacturing textile-reinforced concrete involves applying a thin layer of cementitious mortar to the textile reinforcement, which is then impregnated with a high-performance cementitious matrix. The fibers' strong bond to

the concrete matrix is ensured by this impregnation, allowing for efficient load transfer between the two materials [14]. The resulting TRC panels or elements can be used in various applications, including architectural facades, cladding, thin-shell structures, and precast elements. TRC offers design flexibility, allowing for thinner and lighter elements compared to traditional concrete, while maintaining or improving structural performance [15,16]. Recently, there has been an increase in interest in the usage of textile-reinforced concrete due to its potential for reducing material consumption, energy consumption during manufacturing, and carbon footprint [17,18]. Additionally, TRC exhibits good durability and fire resistance properties, making it an attractive choice for sustainable construction practices [19–22]. Based on the kind of fibers utilized for reinforcement and the arrangement of the textile reinforcement, there are various types of textile-reinforced concrete (TRC) [23–27]. Fibers generally come in two types: natural and artificial. Animals, plants, and natural minerals are the primary sources of natural textile fibers; in contrast, man-made materials include ceramics and synthetic materials made with mineral fibers [28]. Jute, flax, bamboo, cotton, sisal, and coir are a few examples of common natural fibers. Table 1 displays man-made fabrics and their characteristics.

Table 1. Types of textile reinforcement.

Types of Textile Fabric	Usage in TRC	Tensile Strength (MPa)	Young's Modulus (GPa)	Characteristics and Applications
Carbon	Abundantly used in TRC	1100–4000	150–235	High ductility, used in shells, slabs, and most structural applications
AR Glass	Next most used in TRC	120–790	30–40	Less ductile than carbon fabric, used in façade panels, formwork, and non-load bearing partition walls
Basalt (with coatings)	Least commonly used in TRC	490–890	28–45	Most sustainable alternative, used in non-structural elements

Additionally, textile reinforcements can be categorized based on their configurations, which include woven fabrics, non-woven fabrics, and grid structures. Woven fabrics consist of interlaced fibers, similar to traditional textiles, while non-woven fabrics have fibers bonded together mechanically or chemically. Grid structures involve the arrangement of fibers in a grid pattern, creating a mesh-like reinforcement. The specific type of TRC chosen depends on the requirements, such as the desired mechanical properties, environmental conditions, and cost considerations. Corrosion of the embedded metals and reinforcing steel is the primary cause of concrete deterioration. As a result, non-corrosive metals are now utilized, such as textile reinforcement. In previous studies, only textile reinforcement, excluding steel reinforcement, was used, and it did not give satisfactory flexural strength compared to conventional beams. In this study, carbon fabric has been chosen as a textile reinforcement to reinforce the concrete partially along with a steel reinforcement to improve the tensile strength of concrete and reduce concrete deterioration. As the reinforcement is placed over the fabric, the foreign ions will first reach the fabric, thus reducing the concrete deterioration. Structural health monitoring (SHM) is an important aspect of evaluating the safety, integrity, and functionality of structures [29]. SHM involves the continuous or periodic monitoring of structural parameters to detect changes, damage, or potential failures in real-time [30,31]. Here are some commonly employed SHM techniques:

Strain Gauges—Strain gauges are frequently employed in structural health monitoring to measure the deformation or strain in structural components such as bridges, buildings, and other infrastructure. Strain gauges are embedded in the surface of the structural component where deformation or strain needs to be monitored. They are often attached

to critical locations, such as areas prone to high stress or where damage is more likely to occur [32,33].

Fiber Optic Sensors—Because of their unique properties, fiber optic sensors have become increasingly common in structural health monitoring, including high sensitivity, resistance to electromagnetic interference, and their ability to cover large areas with distributed sensing. Fiber Bragg grating sensors and distributed fiber optic sensors are most commonly used [34,35].

Acoustic emission sensors are strategically placed on or within the structure being monitored. These sensors are sensitive to the high-frequency stress waves produced by structural changes [36–38].

Electromagnetic techniques are employed in structural health monitoring to assess the condition of structures by utilizing electromagnetic waves and their interactions with the materials. These techniques are non-destructive and can provide valuable information about the integrity and potential damage of structures [39–41].

Ultrasonic techniques are widely used in structural health monitoring to assess the condition of materials and structures by utilizing ultrasonic waves. Ultrasonic methods are non-destructive and can provide valuable information about the integrity, thickness, and potential defects within structures [42–44].

The choice of monitoring technique depends on factors such as the specific application, accessibility of the structure, required sensitivity, and desired level of monitoring coverage. Developing a comprehensive monitoring strategy tailored to the structure's characteristics and anticipated failure modes to ensure an effective and reliable assessment of the structure's health is important. Generally, sensors are bonded to the surface of the structure or embedded within the concrete during construction. In this study, strain gauges were used to monitor the stress–strain behavior of the carbon fabric-reinforced concrete beam.

2. Design and Properties of Materials

2.1. Textile

The carbon fabric, produced by Taishan Company in Mumbai, was the textile employed in this study. As shown in Figure 1, carbon fabric was woven along the warp and weft direction. Table 2 shows the properties of the carbon fabric mesh.

Figure 1. Carbon fabric mesh.

Table 2. Mechanical properties of the carbon fabric mesh.

Properties		Values
Woven pattern		Plain
Linear Density	Warp g/cm^3	4.5
	Weft g/cm^3	4.5
Thickness(mm)		0.28
Area weight (g/m^2) ± 10%		200
Tensile strength (Mpa)		3530
Modulus in tension (GPa)		230
Elongation %		1.5

2.2. Tensile Test of Carbon Fabric

Carbon fabric was impregnated with epoxy coating to activate more internal filaments, which improves the load transfer between the filaments. Samples were taken in weft and warp direction to test the horizontal and vertical tensile load and its elongation force. Each sample was clamped in the jaws of the tensile strength tester machine in the required direction. The gauge length was about 300 mm, and the test speed was about 2 mm/min. The load was applied slowly for about 2 mm/min until its elongation break point, as depicted in Figure 2.

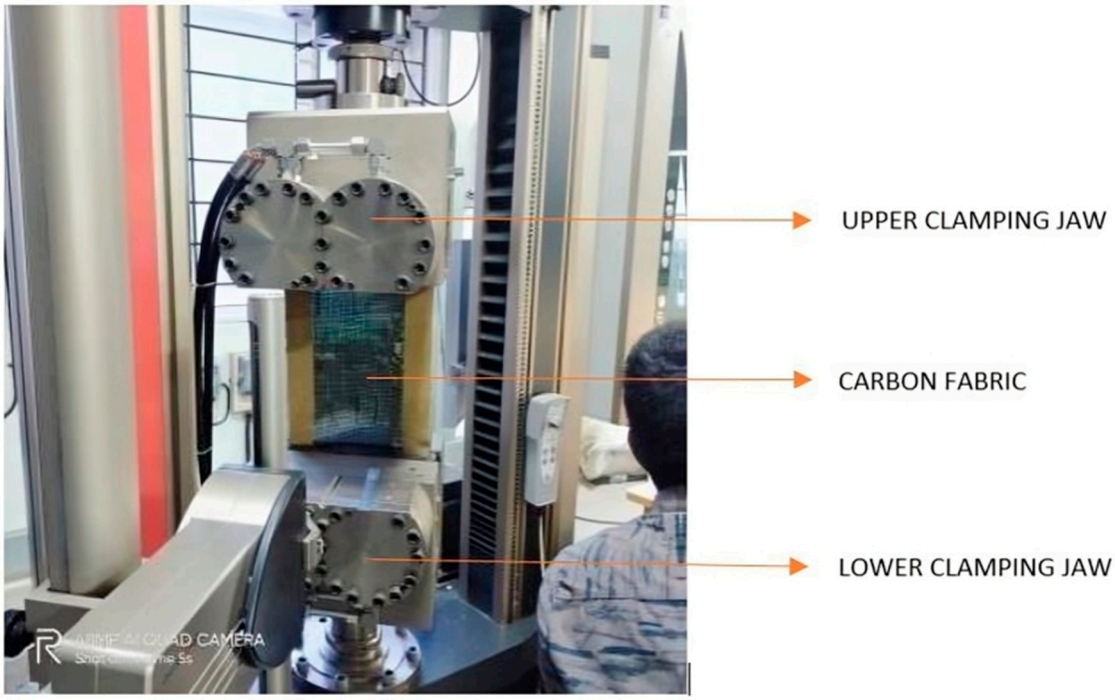

Figure 2. Tensile testing of carbon fabric.

Figure 3 displays the stress–strain curve of the fabric sample that was recorded in both the warp and weft directions. Table 3 displays the test findings. From the graph, it is observed that both the specimens tested in the weft direction record a maximum tensile stress of 104 MPa and the specimens tested in the warp direction record a maximum tensile stress of 44.3 MPa and 40.9 MPa, respectively. It is also visible that the carbon fabric has linear elastic behavior.

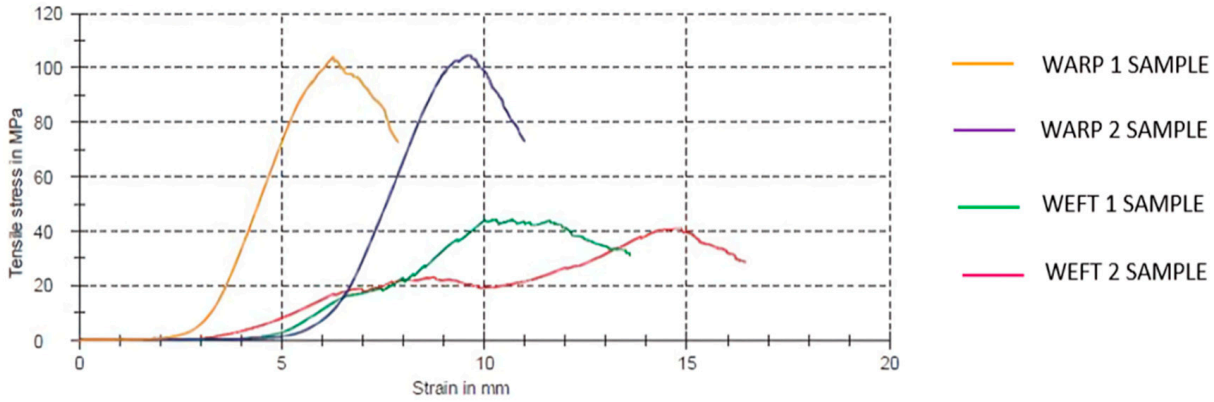

Figure 3. Stress–strain curve of carbon fabric.

Table 3. Tensile properties of the fabric in warp and weft direction.

No.	Specimen ID	P (kN)	S (MPa)	ε Vat Failure %
1	WARP 1	8.18	40.9	5.5
2	WARP 2	5.54	44.3	4.5
3	WEFT 1	13.1	104	3.7
4	WEFT 2	13.0	104	2.6

2.3. Concrete

Ordinary Portland Cement 53 grade (OPC) conforming to IS: 12269-2013 (https://law.resource.org/pub/in/bis/S03/is.12269.2013.pdf, accessed on 4 July 2024) was used for the tests. M-Sand that conformed to the specifications of IS 383-1970 (https://law.resource.org/pub/in/bis/S03/is.383.1970.pdf, accessed on 5 July 2024) was used. Coarse aggregate that conformed to the specifications of IS 383-1970 was used. The specific gravity of the fine aggregates (FAs) and 10 mm coarse aggregates (CAs) was found to be 2.56 and 2.74, respectively. The specific gravity of the cement was found to be 3.15. Both the textile-reinforced concrete (TRC) and reinforced concrete (RC) beam specimens were cast using a concrete mix design with a target compressive strength of 30 MPa. Three standard cubes measuring 150 × 150 × 150 mm^3 were cast and tested at 28 days under compression. The concrete's average compressive strength at 28 days was 35.97 N/mm^2. The concrete mix proportioning for a design compressive strength of 30 MPa is shown in Table 4.

Table 4. Mix proportion of concrete.

Component	Quantity (kg/m^3)
Cement	376
Fine aggregate	873.27
Coarse aggregate	996.4
Superplasticizer	3.76
Water	158

2.4. Pull Out Test

To ascertain the strength of the bond between the concrete and the carbon fabric, a pull out test was performed. Four thin panel specimens measuring 250 × 100 × 10 mm^3 were strengthened by a single layer of epoxy-coated carbon fabric placed in the center based on the test requirements, as shown in Figure 4.

Figure 4. Pull out test specimen.

The defined embedment length was 500 mm. The fabric was axially pulled from the specimen and the load applied was at the rate of 5 mm/min. The results recorded are shown in Figure 5. The mean value of the maximum force recorded was 1270 N and the maximum strain recorded was 2.9 mm. The results show that because of the increased stiffness that the epoxy coating to the carbon fabric gave it, the fabric had a better bond strength with the concrete and less active slip. The linear response signifies the perfect bond between the fabric and the concrete matrix.

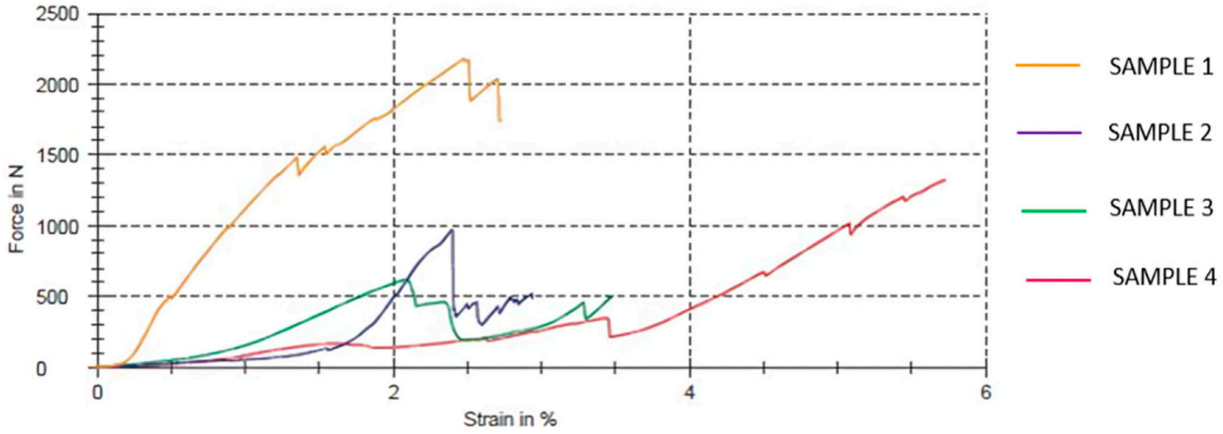

Figure 5. Force versus strain graph for pull out test of carbon fabric.

2.5. Test Specimen

The beam specimen's dimensions were 150 mm in depth, 100 mm in width, and 1000 mm in total length. An epoxy resin coating was applied to the carbon fabric and allowed to cure for 24 h. Fabrics were coated with epoxy to influence the stiffness and draping characteristics. Figure 6 shows the step-by-step casting procedure.

The cast beams were left to set for 24 h. After the setting period, the molds were removed and the beams were immersed in a curing tank and allowed to cure for 28 days. The number of fabric layers and the amount of steel reinforcement (Ast) were chosen as variables to compare the flexural behavior of TRC beams. A total of 3 control beams and 27 TRC beams were cast by partially replacing the steel reinforcement (25%, 50%, and

75%) with 1, 2, and 3 layers of epoxy-coated carbon fabric. Figure 7 shows the detailing of conventional reinforced concrete beams, and Table 5 shows the list of beams cast and their test ID.

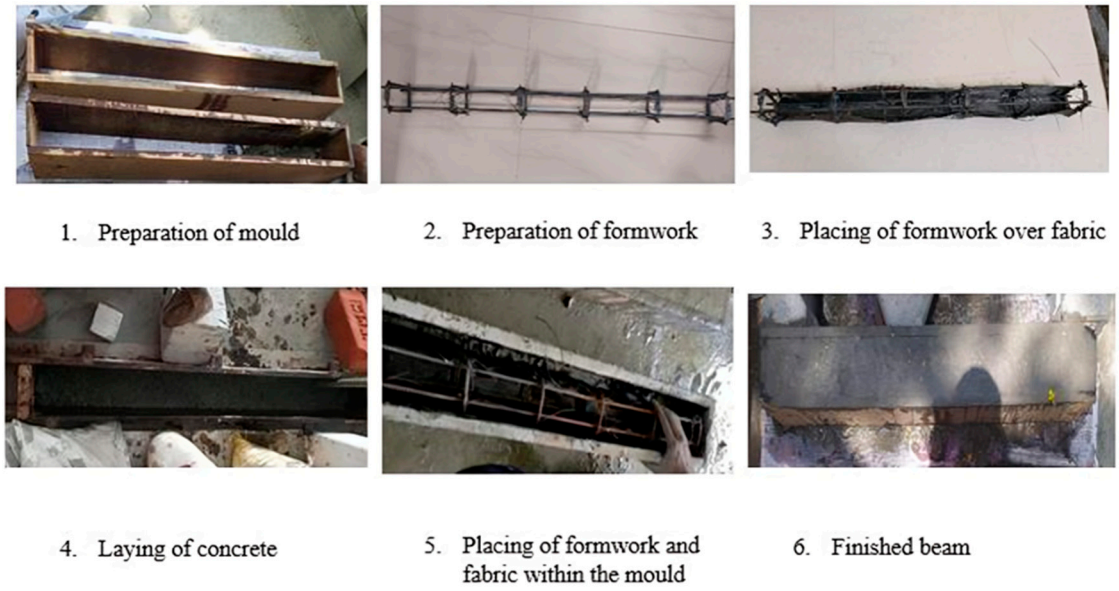

Figure 6. Step-by-step casting procedure.

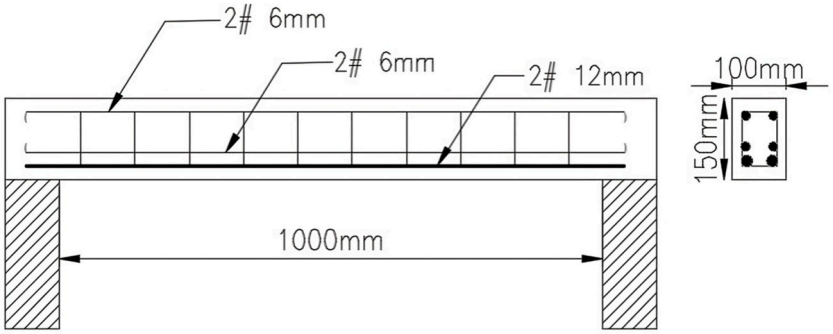

Figure 7. Conventional reinforced concrete beam detailing.

Table 5. Test ID of specimens.

Sr. No	Beam Designation	Percentage of Steel Reinforcement	Number of Carbon Fabric Layers
1	Control	100%	NA
2	75% Ast + 1L	75%	1 layer
3	75% Ast + 2L	75%	2 layers
4	75% Ast + 3L	75%	3 layers
5	50% Ast + 1L	50%	1 layer
6	50% Ast + 2L	50%	2 layers
7	50% Ast + 3L	50%	3 layers
8	25% Ast + 1L	25%	1 layer
9	25% Ast + 2L	25%	2 layers
10	25% Ast + 3L	25%	3 layers

3. Test Setup

Four-point bending tests were carried out to extensively evaluate the beams' flexural behavior. The beams were tested using a loading frame. The load deflection behavior, maximum load-carrying capacity, and beam crack pattern were studied in the experiments. The effective span of the beam was 800 mm. To monitor the stress–strain characteristics, four numbers of 120 ohms 30 mm strain gauges were pasted using bonding adhesive at four different locations, as shown in Figure 8. Before pasting the strain gauges, the surface of the beams was cleaned.

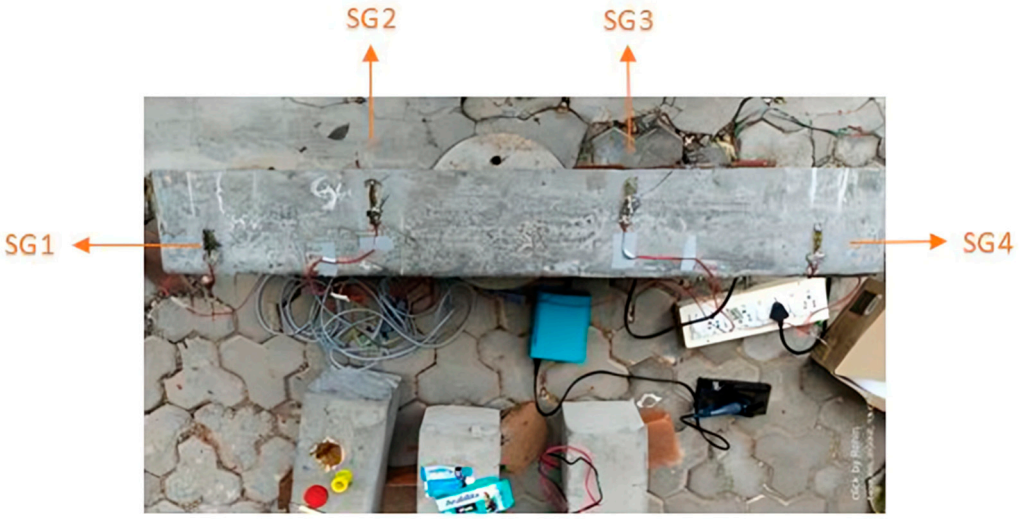

Figure 8. Pasting of strain gauges on the surface of beam.

Three LVDTs placed at the left end, center, and right end were used to monitor the deflection of the beams. White paint was applied to the test area to make it easier to observe the way cracks developed and propagated. The reading was obtained at consistent load intervals. The specimen was visually examined, and cracks were noted while it was being loaded. At regular intervals, pictures were taken to properly capture the crack pattern during testing, and this is depicted in Figure 9.

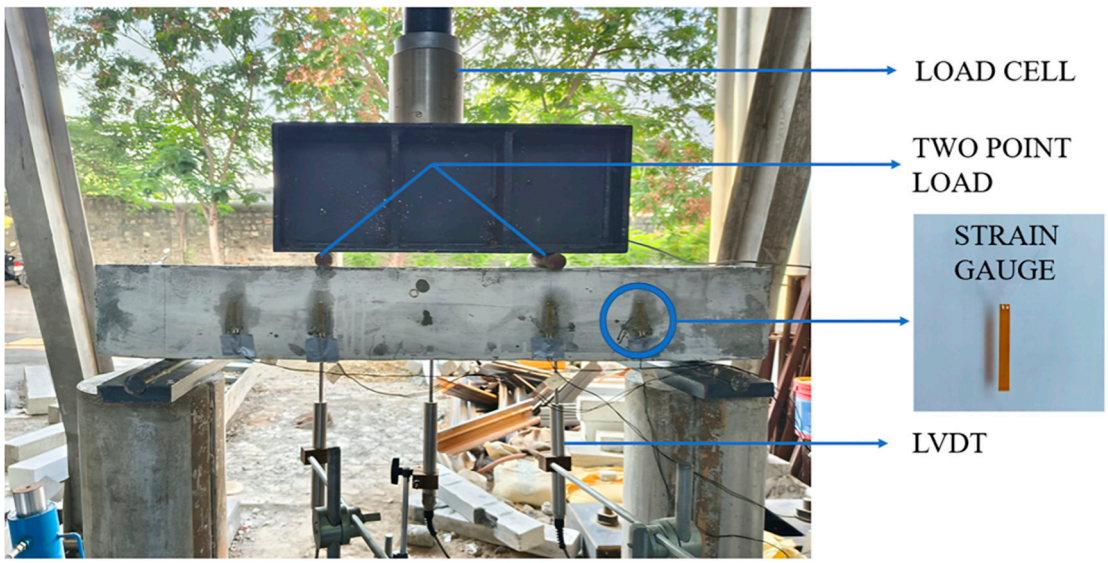

Figure 9. Testing of beams.

4. Analytical Study of Conventional and TRC Beams

To validate the results of the experimental investigation, finite element (FE) modeling of the control and TRC beams was carried out. The general-purpose finite element modeling software ABAQUS (2017, Simulia, Johnston, RI, USA) was used to simulate the beams numerically. The various items concerned with modeling were addressed as follows: element type, specify boundary conditions, material assigning property, loading conditions, meshing operations, and assigning sections; finally, result analysis was performed to complete the entire analytical process. Deformable solid extrusion and shell planar modeling were used for the concrete and laminate modeling. Three-dimensional deformable wire planar modeling was used for the reinforcement. The measured material properties were used in the finite element model. The homogenization in beam dynamics has been extensively studied for heterogeneous material [45].

5. Test Results and Discussion

5.1. Flexure Strength of Beams

The test results summary for all the beams tested is shown in Table 6. The ultimate load-carrying capacity of the control beam was 44.3 kN from the experimental investigations. It was observed that 50% and 25% steel-replaced beams with carbon fabrics performed better than the control beams. However, 75% of steel-replaced beams did not show significant improvement in flexure strength. The ultimate load-carrying capacity of 50% steel-replaced beam with one-layer carbon fabric and 25% steel-replaced beam with one-layer carbon fabric was 52 kN and 70 kN, respectively. The ultimate load-carrying capacity of the TRC beams increased with an increase in the number of fabric layers. The results obtained by testing both the conventional and partially steel-replaced carbon fabric-reinforced concrete beams for flexure strength are shown in Figure 10.

Table 6. Test matrix.

Sr. No	Beam Designation	Ultimate Load (kN)	Mid Span Deflection at Ultimate Load (mm)
1	Control	44.3	4.01
2	75% Ast + 1L	70	6.22
3	75% Ast + 2L	83.2	3.08
4	75% Ast + 3L	90.8	2.05
5	50% Ast + 1L	52	8.32
6	50% Ast + 2L	54	4.65
7	50% Ast + 3L	60.6	3.42
8	25% Ast + 1L	28	9.8
9	25% Ast + 2L	36	5.7
10	25% Ast + 3L	40	4.95

From the graph, it is evident that the flexural strength is directly proportional to the increase in the number of fabric layers. In addition, the partial replacement of steel reinforcement with 50% and 25% carbon fabric beams performed better than conventional beams. Based on the cost analysis carried out, it is apparent that 50% partial replacement of steel reinforcement with one-layer carbon fabric beam is more advantageous than other TRC beams.

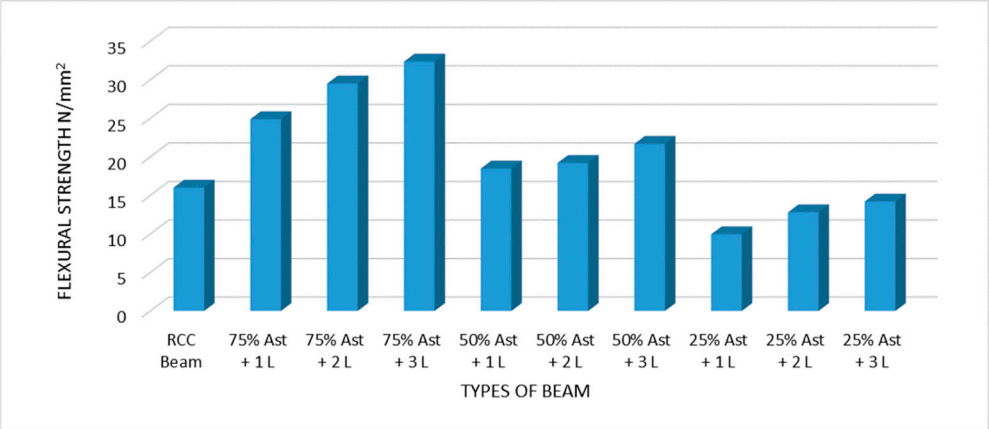

Figure 10. Flexure strength of beams.

5.2. Crack Pattern of TRC Beam

Crack patterns were carefully observed throughout the loading process. Diagonal tension failure started due to the development of a vertical crack at the bottom of the beam due to flexural tensile stress. Then, as the beam's load increases, the fracture grows longer and wider, bending diagonally and advancing toward the upper section of the beam and the loading point. Additionally, sudden failure of concrete in shear happens during the final stage of shear tension failure. Figure 11 shows the crack pattern developed in 50% steel replaced with a one-layer carbon fabric beam.

Figure 11. Crack pattern developed in TRC beam.

5.3. Load Deflection Behavior

From the flexure strength results, 50% steel provision with one layer of carbon fabric and 75% steel provision with one layer of carbon fabric were identified as optimum beams. The load deflection curves for the conventional beam and optimum beams are shown in Figures 12–14. On a general note, from all three curves, it is visible that the deformation increases as the load increases gradually, which results in the widening of the crack widths, and many cracks were observed as the load increased. In the control beam, the first crack

was observed at 18.2 kN. After the initiation of the first crack, the load-carrying capacity of the beam did not reduce. Immediately after the initiation of the first crack, other cracks also propagated at regular intervals of the load. From Figure 12, it is evident that maximum deflection was recorded in all three LVDTs at an ultimate load of 44.3 kN. By comparing the deflection data, it was seen that LVDT 2 (placed at the center side) showed a maximum deflection of 4.01 mm.

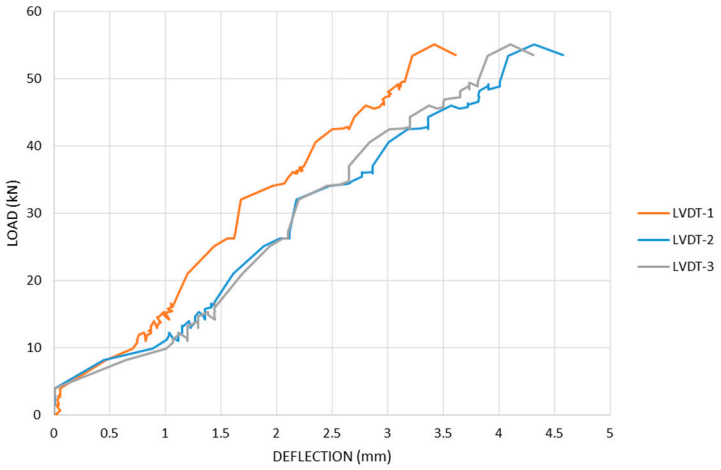

Figure 12. Load deflection curve for conventional beam.

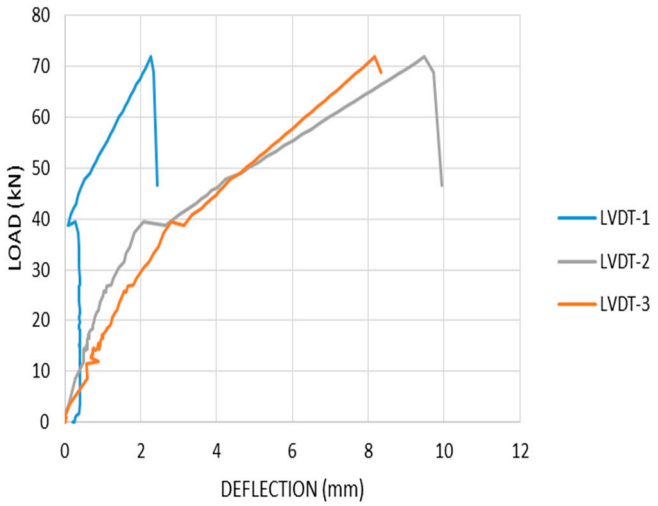

Figure 13. Load deflection curve for 75% Ast + 1 layer carbon fabric beam.

In the 75% Ast + 1 layer carbon fabric beam, the first crack was observed at 30.8 kN. Figure 13 depicts that maximum deflection was recorded in all three LVDTs at an ultimate load of 70 kN. By comparing the deflection data, it was seen that LVDT 2 (placed at the middle side) showed a maximum deflection of 6.22 mm.

In the 50% Ast + 1 layer carbon fabric beam, the first crack was observed at 20.4 kN. From Figure 14, it is seen that maximum deflection was recorded in all three LVDTs at an ultimate load of 52 kN. By comparing the deflection data, it was observed that LVDT 3 (placed on the right side) showed a maximum deflection of 9.64 mm.

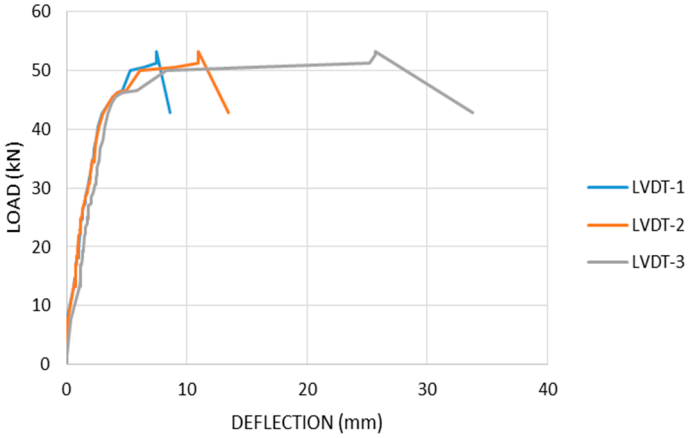

Figure 14. Load deflection curve for 50% Ast + 1 layer carbon fabric beam.

5.4. Analytical Study of TRC Beams

The complete geometry of the control beam, 50% and 25% steel replaced with one-layer carbon fabric beams, and their experimental setup were modeled using ABAQUS software to compare the deflection characteristics of the beam to the experimental results. A 1000 × 100 × 150 mm^3 concrete beam was constructed using a 3D deformable solid extrusion type. In order to develop a concrete beam, an eight-node continuum solid element was utilized. It was created by C3D8R. The element has eight nodes with three degrees of freedom at each node—translations in the nodal x, y, and z directions. A mesh size of 15 mm was used based on the mesh convergence scale. Shell element was utilized to develop carbon fabric. It was created by SC8R. It is a three-dimensional eight node shell element. A mesh size of 10 mm was used based on the mesh convergence scale. To develop steel reinforcement, beam element, was used. It was developed by B31. It is a two-node beam element. Based on the mesh convergence scale, a mesh size of 5 mm was used. The concrete, steel, and fabric properties were listed under material properties. Two-point loading was applied using the interaction module, and the analysis was performed. The deflection models created for control and TRC beams are shown in Figures 15–17.

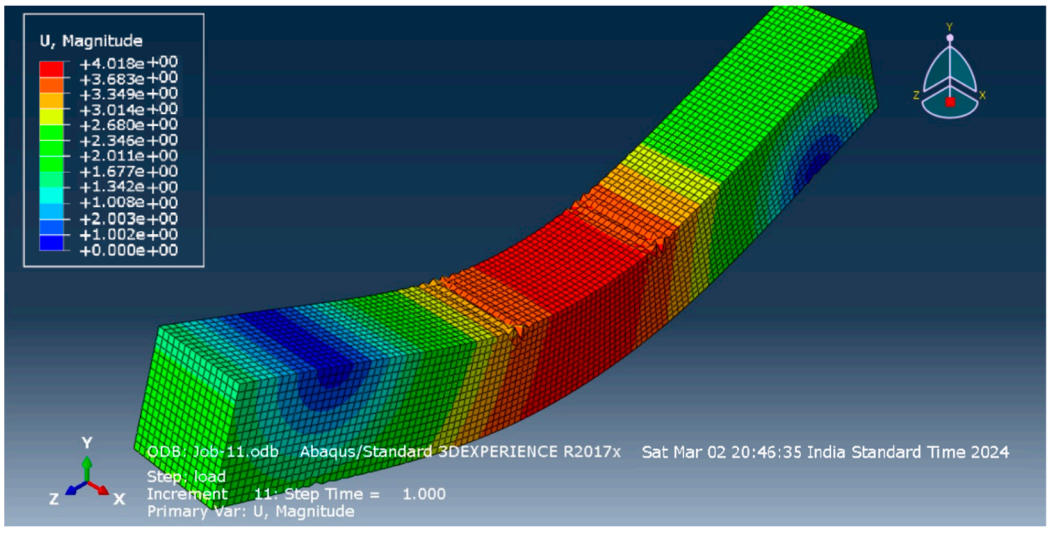

Figure 15. Deflection model of control beam—all dimensions are in mm.

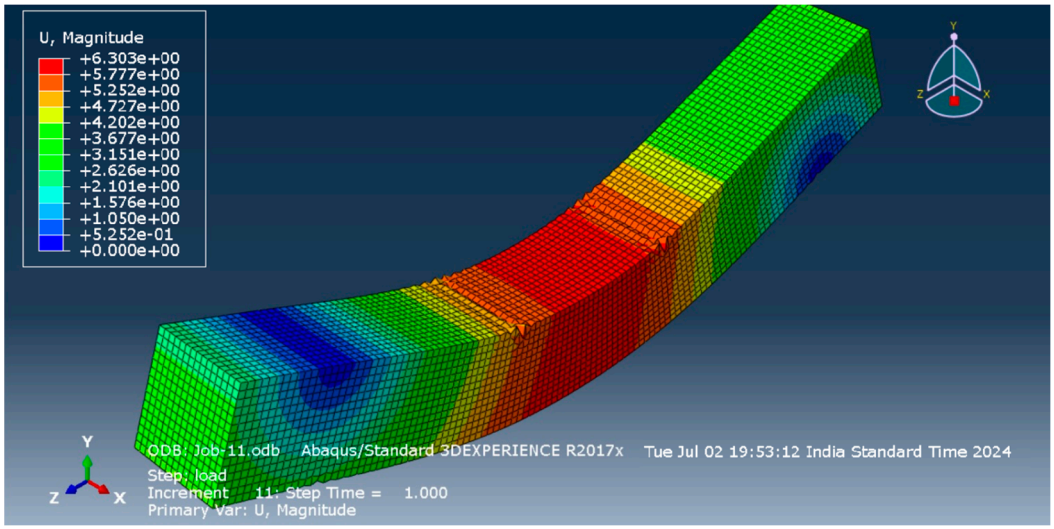

Figure 16. Deflection model of 75% Ast + 1 layer carbon fabric beam—all dimensions are in mm.

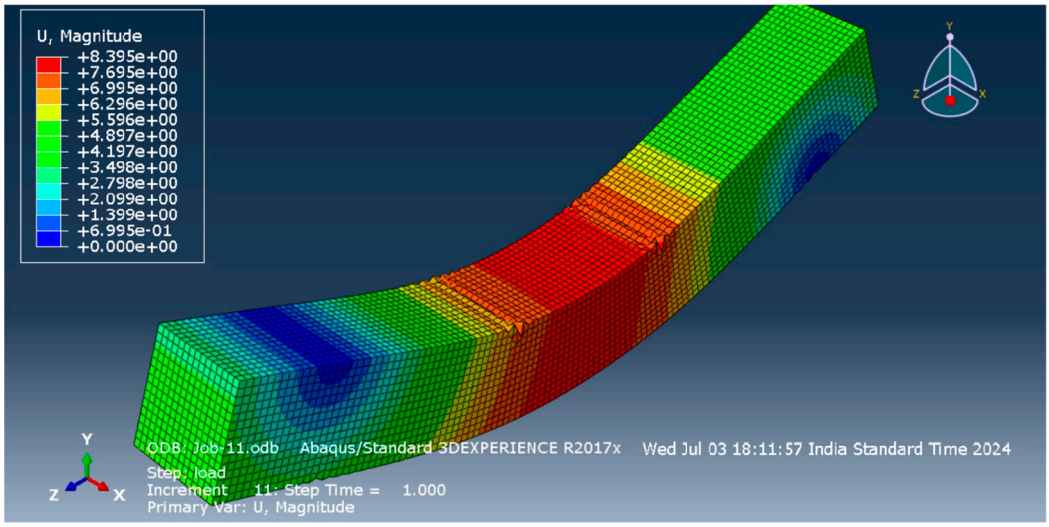

Figure 17. Deflection model of 50% Ast + 1 layer carbon fabric beam—all dimensions are in mm.

Mid-span deflection showed a reasonable agreement between the numerical and experimental results, as summarized in Table 7. As shown in Table 7, compared with the experimental results, a maximum deviation of 0.19% to 1.33% was found for the numerical results for mid-span deflection, respectively.

Table 7. Experimental versus numerical study comparison.

Beam Designation	EXP	FEM	% Difference
Control beam	4.01	4.018	0.19
75% Ast + 1 layer carbon fabric	6.22	6.303	1.33
50% Ast + 1 layer carbon fabric	8.32	8.395	0.90

Figures 18–20 compare the load versus deflection curves for the tested beam specimens derived from the numerical studies and the experimental investigation.

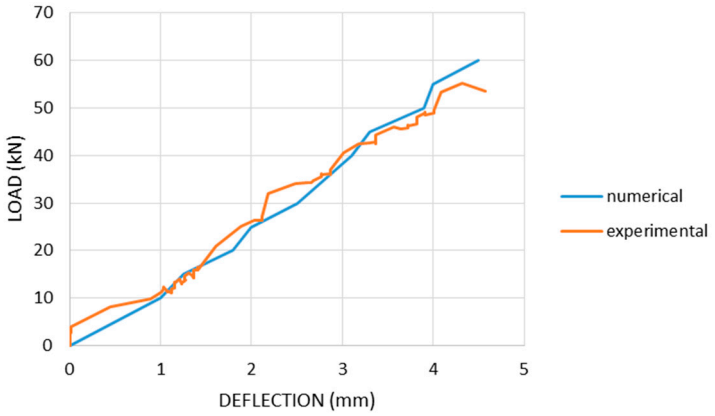

Figure 18. Comparison between numerical and experimental load deflection curve for control beam.

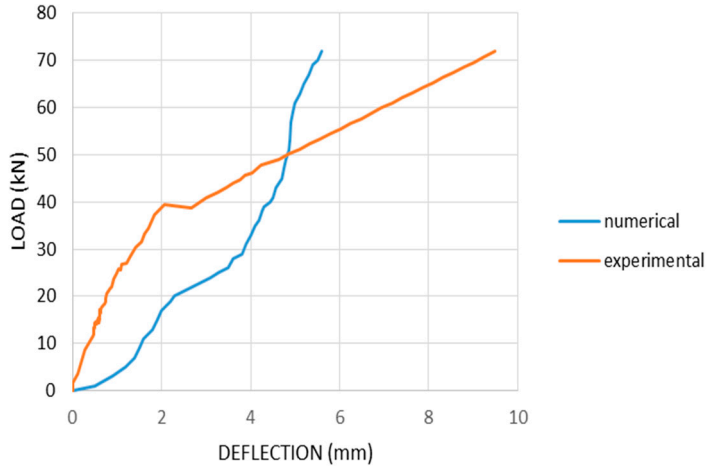

Figure 19. Comparison between numerical and experimental load deflection curve for 75% Ast + 1 layer carbon fabric beam.

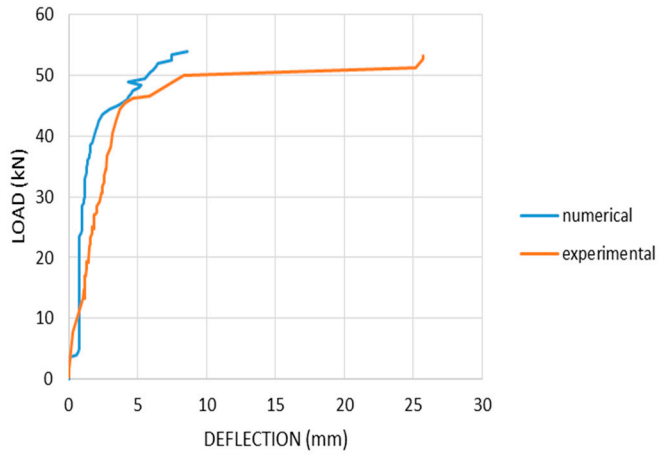

Figure 20. Comparison between numerical and experimental load deflection curve for 50% Ast + 1 layer carbon fabric beam.

5.5. Stress–Strain Characteristics

To monitor the stress–strain characteristics of the beam, four numbers of 30 mm 120 ohm strain gauges were used. Figures 21–23 show the stress–strain curve for the control beam and TRC beams. Overall, the stress–strain curve showed a linear relationship in all the beams. The strain gauge near the left support (SG1) in the control beam recorded

the maximum strain of 111 mm/mm. The strain gauge placed near the left support (SG1) recorded the maximum strain of 83 mm/mm for 75% steel-provided carbon fabric-reinforced concrete beam. In 50% steel-provided carbon fabric-reinforced concrete beam, the strain gauge placed near the right load (SG3) recorded the maximum strain of 96 mm/mm. The carbon fabric-reinforced concrete beams experienced less strain than the conventional beam.

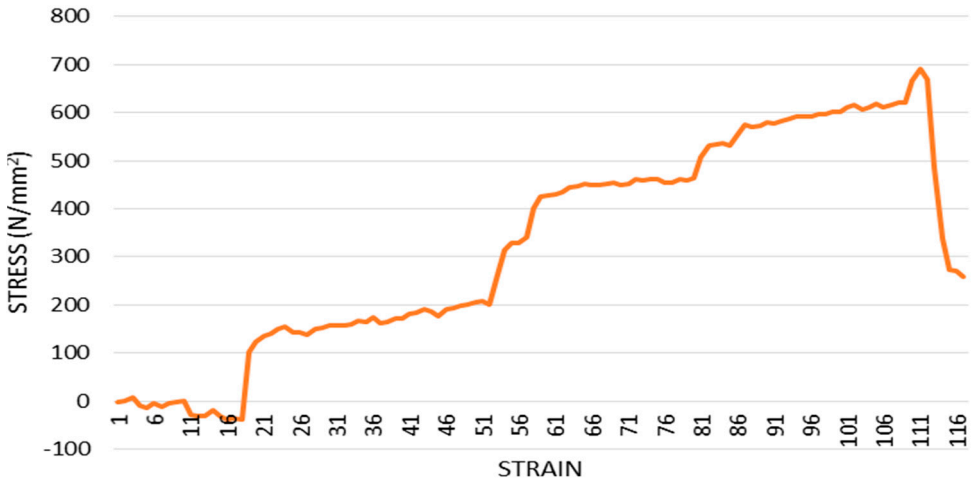

Figure 21. Stress–strain curve for conventional beam.

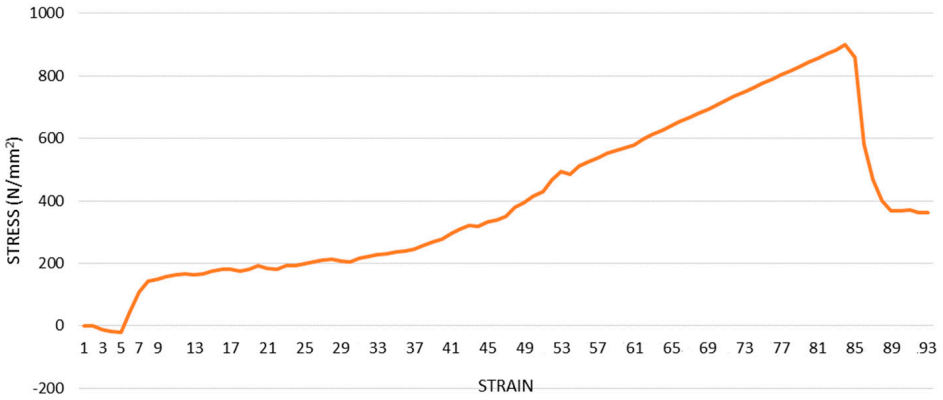

Figure 22. Stress–strain curve for 75% Ast + 1 layer carbon fabric beam.

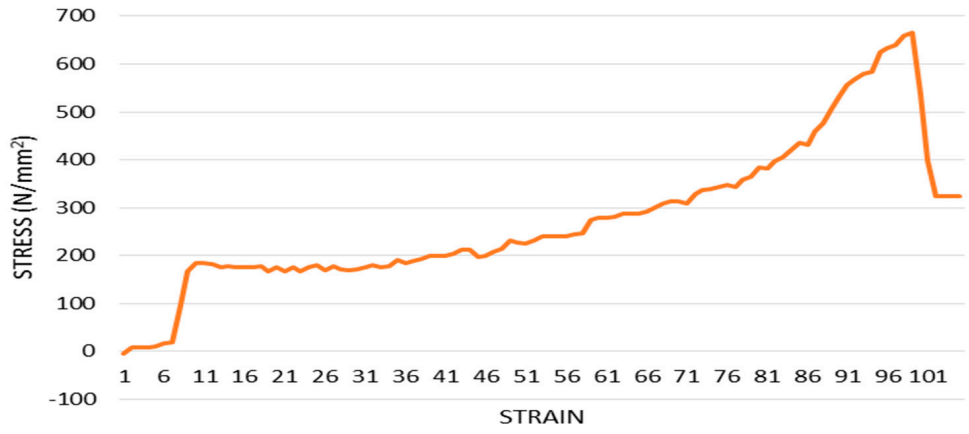

Figure 23. Stress–strain curve for 50% Ast + 1 layer carbon fabric beam.

6. Prediction Model to Determine the Ultimate Load of TRC Beams by ANN

Artificial Neural Networks (ANNs) are extensively used in predictive analysis due to their ability to learn complex patterns and relationships from data. ANNs are versatile and can be applied to various predictive analysis tasks, including regression, classification, time-series forecasting, and pattern recognition. Collecting relevant data is the first step in predictive analysis. Raw data often need preprocessing before being fed into an ANN. Identifying and selecting relevant features are crucial for the performance of an ANN. Too many irrelevant or redundant features may lead to overfitting, while too few features may result in poor predictive performance. Designing the architecture of the neural network involves finding the number of layers, the number of neurons in each layer, the activation functions, and the overall structure of the network. During the training phase, the ANN learns from the historical data to identify patterns and relationships. After training, the ANN's performance is assessed using validation and testing datasets. Once the ANN demonstrates satisfactory performance, it can be deployed for making predictions on new, real-world data [46,47]. In this research, an ANN is used to predict the load-carrying capacity of partially replaced carbon fabric-reinforced concrete beams by taking the steel reinforcement percentage and number of fabric layers as variables. From the experimental investigations carried out, datasets were taken to carry out the predictive analysis.

6.1. Random Forest Regression Algorithm

A versatile machine learning method for predicting numerical values is called random forest regression. The random forest regressor prediction class implements a random forest regression model using the sklearn random forest regressor. This ensemble learning technique works by building a large number of decision trees during training. The mean or average prediction made by each tree is returned for regression tasks. Many decision trees are trained on random subsets of the training data using a technique called bagging. This introduces randomness into the model and reduces overfitting. When splitting nodes during tree construction, only a random subset of features is considered. This further decorrelates the individual trees to improve performance. Combining multiple decision trees produces a more robust and accurate model compared to a single decision tree [48].

6.1.1. Training of Random Forest Regression Algorithm

Training in random forest regression refers to the process of building a random forest model to predict continuous numeric values (regression) based on input features. Random forest algorithms have three main hyperparameters which need to be set before training. These include node size, the number of trees, and the number of features sampled. From there, the random forest classifier can be used to solve regression. The train_data_points() method generates some dummy input feature data X and target values y to train the model. The RandomForestRegressor.fit() method is used to train the regressor on these data.

6.1.2. Prediction of Random Forest Regression Algorithm

Once the model is trained and validated, it can be used to make predictions on new, unseen data by inputting the features of the new data into the trained model, which will then output the predicted target values. A random forest regression model combines multiple decision trees to create a single model. Each tree in the forest builds from a different subset of the data and makes its own independent prediction. The final prediction for the input is based on the average or weighted average of all the individual trees' predictions. For making predictions on new data, get_predic_input_value() reads in a CSV file uploaded and returns the input feature data. predict_output() feeds these data into the trained random forest regressor model to generate predictions. The forest's predictions are averaged to produce the final predicted regression value.

6.1.3. Visualization of Random Forest Regression Algorithm

Visualization involves various techniques used to gain insights into the trained model, understand its behavior, and interpret its results. Visualization techniques are essential for understanding and interpreting the behavior of a random forest regression model, identifying potential issues such as overfitting or underfitting, and gaining insights into the relationships between features and the target variable. create_dataframe() packages the predictions with the original input data into a Pandas DataFrame. Graph() generates a scatter plot of the training data and adds the new prediction point. This allows for visualization of how the prediction relates to the original training data distribution. A scatter plot of random forest regression prediction is shown in Figure 24.

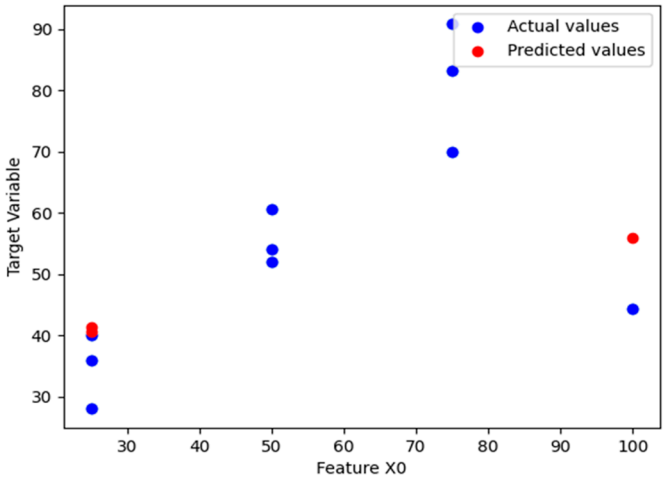

Figure 24. Scatter plot of random forest regression prediction.

6.2. Support Vector Machine (SVM) Regression

The SVM prediction class implements a support vector regression model using Sklearn's SVR.VM regression aims to find the hyperplane (defined by support vectors) that best fits the training data while maximizing the flatness of the mapping. This makes the method robust and less prone to overfitting. SVR maps inputs to a high-dimensional feature space, where a linear regression is carried out, using a kernel trick. Common kernels include radial basis function and polynomial kernels. A tube with radius e is added around the fitted hyperplane to tolerate some prediction errors and prevent massive overfitting. This tube constraint controls model flexibility. Only support vectors that define the hyperplane margins influence the prediction. Data points inside the tube do not.

6.2.1. Training of SVM Regression

Training in support vector machine (SVM) regression involves the process of fitting a model to a dataset in order to learn the relationship between input features and continuous target variables. Training in SVM regression involves finding the optimal hyperplane that best fits the training data while maximizing the margin and minimizing prediction errors. train_data_points() generates dummy input feature data X and target values y. SVR.fit() fits the regression model on this training data. Key hyperparameters like C, epsilon, and kernel parameters control model behavior.

6.2.2. Prediction of SVM Regression

Prediction in SVM regression involves applying the learned model to new data points to estimate the continuous target variable and assessing the performance of these predictions to understand the model's accuracy and reliability. To make predictions, the values of the features for the new data point are input into the trained SVM regression model. The model then applies the learned decision function to these feature values to estimate

the continuous target variable. get_predic_input_value() obtains new input data from the uploaded CSV. predict_output() feeds these data into the trained SVR model to generate predicted values. The position of the new data relative to the tube and support vectors determines the prediction.

6.2.3. Visualization of SVM Regression

Visualization in support vector machine (SVM) regression can be challenging compared to classification tasks, as the output is a continuous variable rather than a discrete class. While visualizing SVM regression models may not be as straightforward as in classification tasks, these techniques can still provide valuable insights into the model's behavior, performance, and the relationships between input features and the target variable. A plot shows the training data distribution and where the new prediction point falls relative to it. This provides insight into the prediction logic for the given inputs. The gradio interface allows for the interactive testing of different input data CSVs to see the prediction performance. The scatter plot of support vector machine regression is shown in Figure 25.

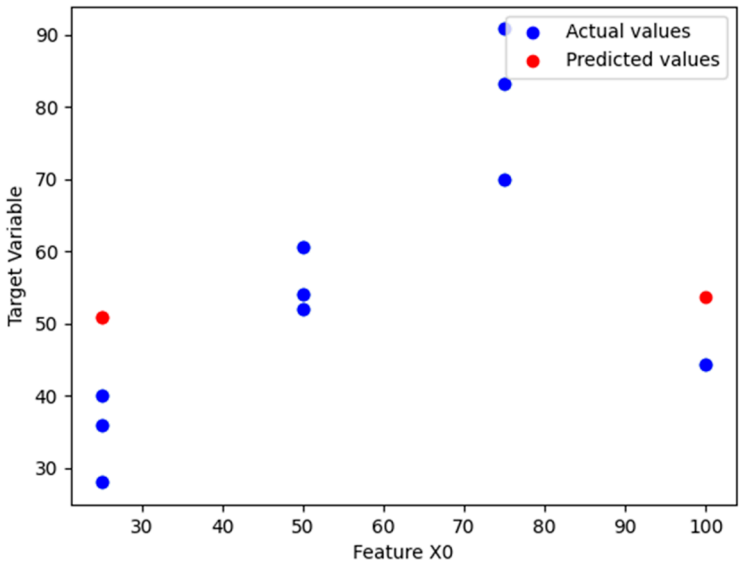

Figure 25. Scatter plot of support vector machine regression.

6.3. Multilayer Perceptron (MLP) Regression

The MLP Regressor Algorithm implements a multilayer perceptron neural network for regression using sklearn's MLP Regressor. This feed-forward ANN model maps inputs to appropriate outputs. It is made up of various node layers, such as an input layer, one or more hidden layers, and an output layer. Each node in one layer connects with a certain weight wij to every node in the following layer.

6.3.1. Training of MLP Regression

Training an MLP regression model involves iteratively adjusting the weights and biases of the network to minimize the difference between the predicted and actual target values, ultimately resulting in a model that can accurately predict continuous variables. The fit() method trains the MLP Regressor on the provided input feature data X and target values y. Backpropagation is used to iteratively adjust weights and biases to minimize the loss between the predicted and actual target values.

6.3.2. Prediction of MLP Regression

Prediction involves using a trained neural network model to estimate the continuous target variable (or response variable) for new, unseen data points based on their input features. To make predictions on new data, get_predic_input_value() obtains new input

data from the uploaded CSV. The trained MLP Regressor generates predicted values by passing new data through the network architecture. Outputs are generated by calculating activations through the network layer by layer.

6.3.3. Visualization of MLP Regression

Visualizing the relationship between each input feature and the target variable can provide insights into their correlation. A scatter plot shows true targets vs. predictions to visually assess performance. The gradio interface allows for interactive testing to gauge prediction accuracy on varying input data. Figure 26 shows the scatter plot of multilayer perceptron regression.

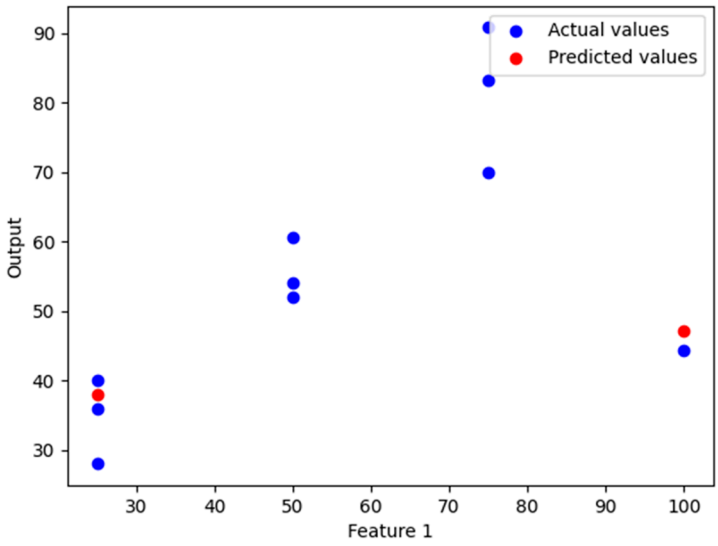

Figure 26. Scatter plot of multilayer perceptron regression.

6.4. XGBoost Algorithm

The XGBoost class implements the XGBoost library for gradient-boosted decision tree regression. This ensemble technique combines multiple decision tree models. Trees are added sequentially, with each new tree correcting errors from the existing sequence. This boosting process reduces bias and variance for improved performance. Regularization helps prevent overfitting as more trees are added.

6.4.1. Training of XGBoost Algorithm

Training in the XGBoost algorithm involves iteratively building decision trees and optimizing them to minimize a specified objective function. Through gradient boosting and regularization techniques, XGBoost produces an ensemble of decision trees that can make accurate predictions for regression tasks. The fit() method trains an XGB Regressor on the provided X input features and the y target variable. Key hyperparameters like n_estimators control ensemble size and performance.

6.4.2. Prediction of XGBoost Algorithm

For prediction, the values of the features for the new data point are inputted into the trained XGBoost model. The model then uses the ensemble of decision trees to generate a prediction for the target variable based on the input features. get_predict_input_values() obtains new input data from the uploaded CSV. The trained model uses the learned tree sequence to generate predictions for this new data. Predictions are made by the weighted summation of outputs from individual trees.

6.4.3. Visualization of XGBoost Algorithm

Visualization in the XGBoost algorithm primarily revolves around understanding the model's structure, feature importance, and decision-making process. A scatter plot can visually assess prediction accuracy and can compare actual vs. predicted values. The gradio interface allows for interactively testing predictions on new input CSVs. Figure 27 shows the XGBoost prediction scatter plot.

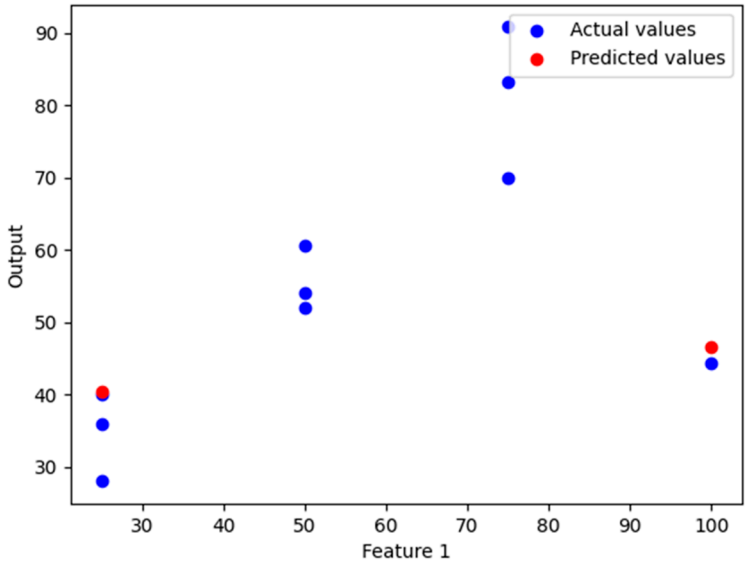

Figure 27. Scatter plot of XGBoost prediction.

6.5. Output

In the prediction model created based on the regression analysis carried out, steel reinforcement percentage and the number of fabric layers are taken as inputs to predict the ultimate load of the TRC beams. Figure 28 shows the prediction model created by ANN.

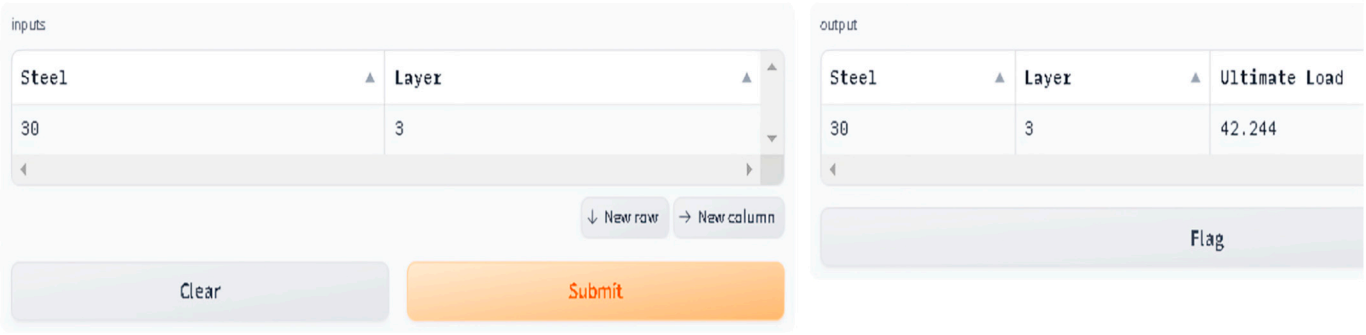

Figure 28. Prediction model created by ANN.

7. Conclusions

This research explores the potential application of carbon fabric as textile reinforcement. Based on the experimental and numerical results reported in this study, the following conclusions are made.

- It is concluded that the flexural behavior of beams can be improved by partially replacing the steel reinforcement with carbon fabric, and the effectiveness depends on the number of fabric layers used.
- Based on the experimental investigation conducted in this research work, compared to control beams, 50% and 75% steel-provided beams proved a significant increase in the flexural capacity of beams with one, two, and three layers of carbon fabrics.

- In accordance with the results of the cost analysis, the optimum level of replacement is identified as 50% steel replacement with one layer of carbon fabric.
- From the crack pattern, it is observed that the beam failed in shear. Hence, shear strengthening of the beam would yield better results.
- The numerical results showed a maximum deviation ranging from 0.19% to 1.33% when compared to the experimental results for mid-span deflection of the control and TRC beams.
- The stress–strain characteristics of the carbon fabric-reinforced concrete beams proved promising by showing a linear elastic response.
- Hence, from the study carried out, it is concluded that carbon fabric can be effectively used as textile reinforcement in beams in addition to steel reinforcement to improve the flexural strength of beams.

Author Contributions: R.M.: Software, Investigation, Formal Analysis, Resources, Writing—Original Draft, Visualization. J.M.J.: Software, Methodology, Resources, Data Curation. M.P. and I.S.K.: Investigation, Resources, Data Curation, Writing—Original Draft, Writing—Review and Editing, Supervision, Project Administration, Funding Acquisition. All authors have read and agreed to the published version of the manuscript.

Funding: This research received no external funding.

Institutional Review Board Statement: Not applicable.

Informed Consent Statement: Not applicable.

Data Availability Statement: Data are contained within the article.

Conflicts of Interest: The authors declare no conflicts of interest.

References

1. Alexander, A.E.; Shashikala, A.P. Sustainability of construction with textile reinforced concrete—A state of the Art. *Mater. Sci. Eng.* **2020**, *936*, 012006. [CrossRef]
2. Park, J.; Kim, T.; You, J.; Hong, S.; Park, S.-K. Flexural strength of alkali resistant glass textile reinforced concrete beam with prestressing. *Int. J. Civ. Environ. Eng.* **2017**, *11*, 988–992.
3. Hegger, J.; Zell, M.; Horstmann, M. *Textile Reinforced Concrete-Realization in Applications*; Tailor Made Concrete Structures—Walraven & Stoelhorst, Ed.; Taylor & Francis Group: London, UK, 2008.
4. Butler, M.; Mechtcherine, V.; Hempel, S. Durability of textile reinforced concrete made with AR glass fibre: Effect of the matric composition. *Mater. Struct.* **2010**, *43*, 1351–1368. [CrossRef]
5. Funke, H.; Gelbrich, S.; Kroll, L. A new hybrid material of textile reinforced concrete and glass fibre reinforced plastic. *J. Mater. Sci. Res.* **2013**, *2*, 96–101. [CrossRef]
6. Yin, S.; Xu, S.; Li, H. Improved mechanical properties of textile reinforced concrete thin plate. *J. Wuhan Univ. Technol. Mater. Sci. Ed.* **2013**, *28*, 92–98. [CrossRef]
7. Peled, A.; Mobasher, B. Effect of processing on mechanical properties of textile-reinforced concrete. *ACI Struct. J.* **2008**, *250*, 85–98.
8. Gayathri, C.N.; Singh, R.; Dhanalakshmi, G. Mechanical behaviour of textile reinforced concrete. *Int. Res. J. Eng. Technol.* **2018**, *5*, 2227–2231.
9. Rempel, S.; Ricker, M. Determination of the material properties of the reinforcement for textile-reinforced concrete elements. *Res. Sq.* **2017**, preprint. [CrossRef]
10. Mishra, R.; Militky, J.; Gupta, N.K.; Pachauri, R.; Behera, B.K. Modelling and simulation of earthquake resistant 3D woven textile structural concrete composites. *Compos. Part B Eng.* **2015**, *81*, 91–97. [CrossRef]
11. Sivakumar, A.; Santhanam, M. Mechanical properties of high strength concrete reinforced with metallic and non-metallic fibers. *Cem. Concr. Compos.* **2007**, *29*, 603–608. [CrossRef]
12. Blunt, J.; Jen, G. Claudia Ostertag; Enhancing corrosion resistance of reinforced concrete structures with hybrid fiber reinforced concrete. *Corros. Sci.* **2015**, *92*, 182–191. [CrossRef]
13. Neves, R.; Felicíssimo, D. Control of Cracking in Textile Reinforced Concrete with Unresin Carbon Fibers. *Materials* **2020**, *13*, 3209. [CrossRef] [PubMed]
14. Zak, J.; Stemberk, P.; Vodička, J. Production of a textile reinforced concrete protective layers with non-woven polypropylene fabric. *Mater. Sci. Eng.* **2017**, *246*, 012054.
15. Schneider, H. *Textile Reinforced Concrete Applications and Prototypes*; RILEM: Paris, France, 2006.
16. Kulas, C.; Solidian. Actual applications and potential of textile-reinforced concrete. In Proceedings of the GRC2015, Radison Blu, Dubai, 19–21 April 2015.

17. Novotna, M.; Kostelecka, M.; Hodkova, J.; Vokac, M. Use of textile reinforced concrete—Especially for facade panels. *Adv. Mater. Res.* **2014**, *923*, 142–145. [CrossRef]
18. Hegger, J.; Curbach, M.; Stark, A.; Wilhelm, S.; Farwig, K. Innovative design concepts: Application of textile reinforced concrete to shell structures. *Struct. Concr. J. Fib.* **2018**, *19*, 637–646. [CrossRef]
19. Bisby, L. Fire resistance of textile fiber composites used in civil engineering. In *Woodhead Publishing Series in Fibre Composites in Civil Engineering*; Woodhead Publishing: Sawston, UK, 2016; pp. 169–185.
20. Raupach, M. *Epoxy-Impregnated Textiles in Concrete Load Bearing Capacity and Durability*; RILEM: Paris, France, 2006.
21. Alma'aitah, M.; Ghiassi, B.; Dalalbashi, A. Durability of textile reinforced concrete: Existing knowledge and current gaps. *Appl. Sci.* **2021**, *11*, 2771. [CrossRef]
22. Butler, M.; Mechtcherine, V.; Hempel, S. Experimental investigations on the durability of fibre–matrix interfaces in textile-reinforced concrete. *Cem. Concr. Compos.* **2009**, *31*, 221–231. [CrossRef]
23. Bhat, S.; Kalthoff, M.; Shroeder, P.; Gries, T.; Matschei, T. Textile reinforced concrete for free-form concrete elements: Influence of the binding type of textile reinforcements on the drapability for manufacturing double-curved concrete elements. In Proceedings of the MATEC Web of Conferences 2022, Purwokerto, Indonesia, 12 October 2022; p. 364.
24. Zargaran, M.; Attari, N.K.; Alizadeh, S. Flexural behavior of high-performance and non-high-performance textile reinforced concrete composites. *Eur. J. Environ. Civ. Eng.* **2023**, *27*, 893–907. [CrossRef]
25. Holcapek, O.; Vogel, F. Bond properties of concrete beams strengthened by AR-glass textile and basalt textile reinforced concrete. *Appl. Mech. Mater.* **2016**, *825*, 7–10. [CrossRef]
26. Hegger, J.; Bruckermann, O.; Voss, S. AR-glass and carbon fibers in textile reinforced concrete—Simulation and Design. *ACI Struct. J.* **2007**, *244*, 57–76.
27. Halvaei, M.; Jamshidi, M.; Latifi, M.; Ejtemaei, M. Experimental investigation and modelling of flexural properties of carbon textile reinforced concrete. *Constr. Build. Mater.* **2020**, *262*, 120877. [CrossRef]
28. Venigalla, S.G.; Nabilah, A.B.; Nasir, N.A.M.; Safiee, N.A.; Aziz, F.N.A.A. Textile—Reinforced Concrete as a structural member: A Review. *Buildings* **2022**, *12*, 474. [CrossRef]
29. Barrias, A.; Casas, J.R.; Villalba, S. Embedded Distributed Optical Fiber Sensors in Reinforced Concrete Structures—A case study. *Sensors* **2018**, *18*, 980. [CrossRef] [PubMed]
30. Bergmeister, K.; Santa, U. Structural Health Monitoring of Concrete Bridges. *Interferom. Speckle Light* **2000**, 633–640. [CrossRef]
31. Habel, W. Structural health monitoring systems for reinforced concrete structures. In *Series in Civil and Structural Engineering*; Woodhead Publishing: Sawston, UK, 2010; Volume 2, pp. 63–94.
32. Choi, H.; Choi, S.; Cha, H. Structural Health Monitoring system based on strain gauge enabled wireless sensor nodes. In Proceedings of the International Conference on Networked Sensing Systems 2008, Kanazawa, Japan, 17–19 June 2008.
33. Santos, F.L.M.D.; Peeters, B.; Lau, J.; Desmet, W.; Goes, L. The use of strain gauges in vibration-based damage detection. *J. Phys.* **2015**, *628*, 012119.
34. Bremer, K.; Wollweber, M.; Weigand, F.; Rahlves, M.; Kuhne, M.; Helbig, R.; Roth, B. Fibre optic sensors for the structural health monitoring of building structures. *Procedia Technol.* **2016**, *26*, 524–529. [CrossRef]
35. Sakiyama, F.I.H.; Lehmann, F.; Garrecht, H. Structural health monitoring of concrete structures using fibre-optic-based sensors: A review. *Mag. Concr. Res.* **2021**, *73*, 174–194. [CrossRef]
36. Nor, N.M. Structural health monitoring through acoustic emission. In *Woodhead Publishing Series in Civil and Structural Engineering*; Woodhead Publishing: Sawston, UK, 2018; pp. 123–146.
37. Behnia, A.; Chai, H.K.; Shiotani, T. Advanced structural health monitoring of concrete structures with the aid of acoustic emission. *Constr. Build. Mater.* **2014**, *65*, 282–302. [CrossRef]
38. Desa, M.; Ibrahim, M.; Shahidan, S.; Ghadzali, N.S.; Misri, Z. Fundamental and assessment of concrete structure monitoring by using acoustic emission technique testing: A review. *IOP Conf. Ser. Earth Environ. Sci.* **2018**, *140*, 012142. [CrossRef]
39. Verma, S.; Madhav, A.V.G.; Duggal, G. Structural health monitoring of concrete structures using electromechanical impedance technique. In Proceedings of the International Conference on Control, Instrumentation and Automation 2013, Tehran, Iran, 28–30 December 2013.
40. Tseng, K.; Wang, L. Smart piezoelectric transducers for in situ health monitoring of concrete. *Smart Mater. Struct.* **2004**, *13*, 1017. [CrossRef]
41. Park, G.; Cudney, H.; Inman, D. Impedance-based health monitoring of civil structural components. *J. Infrastruct. Syst.* **2000**, *6*, 153–160. [CrossRef]
42. Hafiz, A.; Schumacher, T. Monitoring of Stresses in Concrete Using Ultrasonic Coda Wave Comparison Technique. *J. Nondestruct. Eval.* **2018**, *37*, 73. [CrossRef]
43. Wiggenhauser, H.; Niederleithinger, E. Innovative Ultrasonic Techniques for Inspection and Monitoring of Large Concrete Structures. In Proceedings of the EPJ Web of Conferences 2013, Varenna, Italy, 30 July–4 August 2012; p. 56.
44. Schickert, M.; Krause, M. Ultrasonic techniques for evaluation of reinforced concrete structures. In *Woodhead Publishing Series in Civil and Structural Engineering*; Woodhead Publishing: Sawston, UK, 2010; Volume 2, pp. 490–530.
45. Gusella, F.; Cluni, F.; Gusella, V. Homogenization of the heterogeneous beam dynamics: The influence of the random Young's modulus mixing law. *Compos. Part B Eng.* **2019**, *167*, 608–614. [CrossRef]

46. Hung, N.T.; Chanh, L.M.; Vuong, D.D.T.; Hung, N.D. Predicting The flexural capacity of corroded reinforced concrete beams using artificial intelligence models. *Tạp Chí Khoa Học Giao Thông Vận Tải* **2022**, *73*, 40–51.
47. Amani, J.; Moeini, R. Prediction of shear strength of reinforced concrete beams using adaptive neuro-fuzzy inference system and artificial neural network. *Sci. Iran* **2012**, *19*, 242–248. [CrossRef]
48. Khan, K.; Iqbal, M.; Salami, B.A.; Amin, M.N.; Ahamd, I.; Alabdullah, A.A.; Arab, A.M.A.; Fazal Jalal, E. Estimating flexural strength of FRP reinforced beam using artificial neural network and random forest prediction models. *Polymers* **2022**, *14*, 2270. [CrossRef] [PubMed]